

# Interplay between hopping and band transport in high-mobility disordered semiconductors at large carrier concentrations: The case of the amorphous oxide InGaZnO

I. I. Fishchuk,<sup>1</sup> A. Kadashchuk,<sup>2,3,\*</sup> A. Bhoolakam,<sup>2,4</sup> A. de Jamblinne de Meux,<sup>2,4</sup> G. Pourtois,<sup>2</sup> M. M. Gavrilyuk,<sup>1</sup> A. Köhler,<sup>5</sup> H. Bäessler,<sup>5</sup> P. Heremans,<sup>2</sup> and J. Genoe<sup>2,4</sup>

<sup>1</sup>*Institute for Nuclear Research, National Academy of Sciences of Ukraine, Prospect Nauky 47, 03680 Kyiv, Ukraine*

<sup>2</sup>*IMEC, Kapeldreef 75, B-3001 Leuven, Belgium*

<sup>3</sup>*Institute of Physics, National Academy of Sciences of Ukraine, Prospect Nauky 46, 03028 Kyiv, Ukraine*

<sup>4</sup>*KU-Leuven, ESAT, Kasteelpark Arenberg 10, 3001 Leuven, Belgium*

<sup>5</sup>*Experimental Physics II and Bayreuth Institute of Macromolecular Research (BIMF), Universitätsstrasse 30, 95448 Bayreuth, Germany*

(Received 25 August 2015; revised manuscript received 2 March 2016; published 13 May 2016)

We suggest an analytic theory based on the effective medium approximation (EMA) which is able to describe charge-carrier transport in a disordered semiconductor with a significant degree of degeneration realized at high carrier concentrations, especially relevant in some thin-film transistors (TFTs), when the Fermi level is very close to the conduction-band edge. The EMA model is based on special averaging of the Fermi-Dirac carrier distributions using a suitably normalized cumulative density-of-state distribution that includes both delocalized states and the localized states. The principal advantage of the present model is its ability to describe universally effective drift and Hall mobility in heterogeneous materials as a function of disorder, temperature, and carrier concentration within the same theoretical formalism. It also bridges a gap between hopping and bandlike transport in an energetically heterogeneous system. The key assumption of the model is that the charge carriers move through delocalized states and that, in addition to the tail of the localized states, the disorder can give rise to spatial energy variation of the transport-band edge being described by a Gaussian distribution. It can explain a puzzling observation of activated and carrier-concentration-dependent Hall mobility in a disordered system featuring an ideal Hall effect. The present model has been successfully applied to describe experimental results on the charge transport measured in an amorphous oxide semiconductor, In-Ga-Zn-O (a-IGZO). In particular, the model reproduces well both the conventional Meyer-Neldel (MN) compensation behavior for the charge-carrier mobility and inverse-MN effect for the conductivity observed in the same a-IGZO TFT. The model was further supported by *ab initio* calculations revealing that the amorphization of IGZO gives rise to variation of the conduction-band edge rather than to the creation of localized states. The obtained changes agree with the one we used to describe the charge transport. We found that the band-edge variation dominates the charge transport in high-quality a-IGZO TFTs in the above-threshold voltage region, whereas the localized states need not to be invoked to account for the experimental results in this material.

DOI: [10.1103/PhysRevB.93.195204](https://doi.org/10.1103/PhysRevB.93.195204)

## I. INTRODUCTION

The advent of a new class of *high-mobility* thin-film semiconductors enables the realization of the next generation of thin-film transistor (TFT) technology and eventually opens a new frontier for large-area electronics called “flexible electronics,” which means electronic circuits fabricated on flexible plastic substrates [1,2]. Since thin films are typically amorphous or polycrystalline, their charge-carrier mobility ( $\mu$ ) is far lower than that measured in perfect single-crystal semiconductors [3]. Nonetheless, a major advantage of amorphous semiconductors is that one can deposit uniform large-area thin films easily at relatively low temperatures, a process that is compatible with plastic substrates. This is a driving motive in this rapidly growing field and an important stimulant for applied and fundamental research. Although the understanding of charge transport is crucial for the realization of high-performance TFTs, its theoretical description is still far from complete. Rather, the description of charge transport in disordered solids with charge mobilities around 1–10 cm<sup>2</sup>/V s, which are relevant for many advanced

organic and amorphous oxide TFTs, is still an unsolved problem. This falls into an intermediate mobility regime where neither the concept of thermally activated hopping transport in low-mobility disordered solids nor the classical band transport model is applicable. A theoretical description of charge transport in this intermediate regime remains a challenge [4].

It is a general notion that disorder, inevitably present in organic as well as in inorganic thin-film semiconductors, lowers the charge mobility significantly. This has an important bearing on the device performance. Structural disorder gives rise to a broad distribution of localized states which include shallow (band-tail) states as well as deep traps. In disordered *organic* solids, all electronic states are localized due to weak intermolecular interaction. Thus, temperature-assisted incoherent hopping through a manifold of localized states, forming a density-of-states (DOS) distribution (typically of Gaussian shape), is the dominant charge transport mechanism. This hopping-type transport was interpreted in terms of the Gaussian disorder formalism, initially introduced by Bäessler and co-workers [5,6] and then extended further by different groups to account for additional important aspects of the transport such as spatial energy correlation effects [7], molecular geometry fluctuations [8], and charge-carrier density effects [9–12]. On the other hand, in conventional *inorganic*

\*Corresponding author: [kadash@iop.kiev.ua](mailto:kadash@iop.kiev.ua)

disordered semiconductors, such as amorphous silicon (a-Si:H), hopping is restricted to low and moderate temperatures [3,13]. This is because the Fermi level is usually located within the distribution of localized electron states. At low temperatures only a few electrons occupy extended states above the mobility edge while most of the electrons are in localized states. Therefore, charge transport is thermally activated and mainly governed by trapping and release processes. The delocalized states above the mobility edge are generally believed to control charge transport only at high enough temperatures, when an essential fraction of charge carriers fills these states [3].

The traditional hopping transport description can become problematic when the Fermi level is very close to the mobility edge. This can happen in heterogeneous systems with a relatively small density of the localized tail states below the mobility edge and at sufficiently large carrier concentrations. Considerable advances were made in the last years in obtaining thin-film semiconductors with greatly improved charge-carrier mobilities exceeding  $1 \text{ cm}^2/\text{Vs}$ . The associated activation energies, defined as the energy difference ( $\Delta$ ) between the Fermi level and the mobility edge, turned out to be as low as  $\sim 10\text{--}40 \text{ meV}$  or even less at sufficiently large gate voltages [14–19]. According to Fermi-Dirac statistics such semiconductor should be degenerated at room temperature as, by definition, degeneration occurs when  $\Delta \leq 3k_B T$  [20]. In this case a large fraction of charge carriers would populate the delocalized states above the mobility edge. Another remarkable characteristic of high-mobility disordered semiconductors is their well-developed free-electron-like Hall effect [14–17,21]. It turns out that the Hall mobility virtually coincides with the drift field-effect transistor (FET) mobility featuring a similar thermally activated behavior. The latter observation is the most intriguing because (i) only delocalized charge carriers can give rise to the ideal Hall effect, and (ii) a temperature-activated Hall mobility ( $d\mu/dT > 0$ ) is incompatible with conventional, i.e., nonactivated, band transport. Obviously, a more advanced model that goes beyond the conventional multiple trap and release (MTR) formalism is needed to describe adequately both the FET and Hall mobilities in these materials.

An approach based on a band transport percolation concept was recently suggested by Kamiya and Nomura [21] to describe thermally activated Hall and drift charge-carrier transport in amorphous oxide semiconductors. The key assumption of the model is that the charge transport occurs via delocalized states in a conduction band with a square-root energy dependence of the DOS, yet with the addition of random potential barriers above the conduction-band edge. These barriers are assumed to have a Gaussian-type distribution, so the manifold of potential barriers in the band can hinder the electrical conduction, especially in low-energy band states. In the Kamiya-Nomura percolation model [21] the effective conductivity in such heterogeneous medium is calculated by averaging the local band conductivity over a specific distribution called “transmission probability” which runs from zero to unity to account for the barrier effect. This is an arguable procedure because it is in variance to established percolation theories based on the percolation threshold that depends on the dimensionality of the system. The Kamiya-Nomura model considers implicitly the conductivity along

an essentially one-dimensional percolative path. However, in such a situation the effective conductivity would be limited by the minimal conductivity at the highest barrier in this path rather than by its average value when the Fermi level is within the energy range of the barrier height variations. Only at large enough carrier concentrations, when the Fermi level exceeds all the barrier heights, the averaging procedure used in [21] might be warranted. The problems related to electrical conductivity calculations in inhomogeneous systems have been thoroughly described by Shklovskii and Efros [22] who demonstrated that averaging of the local conductivity yields a significantly overestimated effective conductivity because it leads to an overestimation of the contribution from regions with high local conductivities. There are actually not enough of high conductive regions to create the infinite percolation cluster enabling conductance in the energetically inhomogeneous system. Besides, we would like to mention that percolation theory is widely accepted as a suitable tool to describe the hopping transport in *strongly* inhomogeneous disordered systems and its applicability to weakly and moderately disordered media is still less justified. For these reasons the application of the Kamiya-Nomura model to the current problem is questionable.

A particularly useful approach for calculating the effective conductivity in moderately and weakly disordered systems can be based upon the effective medium approximation (EMA) method [23], notably since it allows accounting for the dimensionality of the system. It should be noted that the analytical EMA approach has been demonstrated to be an efficient theoretical tool for studying charge transport properties in hopping transport systems [12,24–27]. It was also found that the use of the so-called transport energy concept reduces the complex phonon-assisted hopping process to essentially a trap-limited transport with a broad distribution of localized states and can be implemented into the EMA formalism to extend its applicability to a stronger disordered system as well.

In the present paper, we suggest an EMA theory which is not restricted to conventional hopping transport. Rather it bridges the gap between hopping and bandlike transport in energetically heterogeneous systems containing delocalized and localized states. It is therefore applicable to describe both drift and Hall charge-carrier mobilities in disordered systems in which charge motion occurs via delocalized states. This EMA model is based on averaging the Fermi-Dirac carrier distributions using a suitably normalized cumulative density-of-state (DOS) distribution that includes both extended (delocalized) and localized states. The key assumption of our model is that, in addition to the tail of localized states distribution, disorder can also give rise to static spatial variation of the conduction-band edge  $\varepsilon_m$ . As will be demonstrated below, it is more appropriate to discuss  $\varepsilon_m$  for the amorphous oxide semiconductors in terms of the conduction-band edge instead of the mobility edge. Both factors can contribute to the temperature- and carrier-concentration dependence of the effective charge-carrier mobility in the system, while their relative contribution is material specific. At low carrier concentration and/or sufficiently strong disorder the charge transport is controlled by the localized states. However, if the density of the localized states is low enough, a degeneration regime can be realized in such heterogeneous system even at moderate

temperatures at a high enough carrier concentration, i.e., when Fermi level is very close to (or above) the transport-band edge. In this limiting case, charge transport will predominantly be controlled by the static variations in the potential landscape of the  $\varepsilon_m$  giving rise to thermally activated drift and Hall mobilities that depend on the carrier concentration. The variation of  $\varepsilon_m$  is assumed to obey a Gaussian distribution [28] with the standard deviation  $\delta_0$ . This closely resembles the idea of a barrier distribution in the conduction band introduced in the Kamiya-Nomura model [21]. In the latter case, however, the Gaussian distribution was centered at an energy offset from the band edge by the average barrier height.

We applied the present theory to describe the charge transport properties in an amorphous metal oxide *n*-type semiconductor—indium–gallium–zinc–oxide (a-IGZO)—used here as a model high-mobility disordered system [2,14,29]. a-IGZO can be considered as an intrinsically disordered solid because the constituting ions are statistically distributed at the lattice sites [2,21,29]. This material has recently attracted a lot of interest because it can possibly replace a-Si:H in applications in backplanes for large-area active matrix displays. It is also a promising semiconductor material for emerging transparent flexible electronics because it is highly transparent in the whole visible range, and has a high charge-carrier mobility and superior spatial uniformity over a wide area due to the absence of grain boundaries. A further advantage is that the films can be fabricated by a conventional sputtering method [14] or a solution based deposition technique [30]. a-IGZO films feature a charge-carrier mobility of  $10 \text{ cm}^2/\text{Vs}$  or more at room temperature [2,14], that is one to two orders of magnitude greater than in a-Si:H films where *typical* FET mobility is about  $0.1\text{--}1.0 \text{ cm}^2/\text{Vs}$  [31,32]. This is due to the fact that the bottom of the conduction band is composed of metal *s* orbitals which are weakly influenced by the amorphization. Therefore the density of localized states is significantly much lower in this material. Remarkably, an a-IGZO film shows a well-developed Hall effect [29,33] suggesting that the mobile charge carriers are actually delocalized and that the length of the electron mean path is much larger than in other amorphous semiconductors. Although the charge mobility is large, both drift FET and Hall mobilities typically feature a thermally activated behavior with an activation energy  $\sim 15\text{--}10 \text{ meV}$  at large gate voltages.

We characterized a high-quality a-IGZO TFT device over a range of temperatures and gate voltages and the experimental results support well our EMA model. Using *ab initio* calculations we (i) confirmed that the electron conduction states are delocalized in a-IGZO, and (ii) found that the amorphism of a-IGZO gives rise to variations of the conduction-band edge rather than to the creation of localized states. The latter are probably of defect origin that is in line with the very low density of the localized states observed experimentally in similar a-IGZO films [34] as compared to other disordered semiconductors. We find that the localized states might not need to be taken into account to describe the transport properties of our advanced a-IGZO TFT devices at sufficiently large gate voltages. It turns out that the only fitting parameter necessary to explain the experimental data in our a-IGZO films is the standard deviation  $\delta_0$  of the conduction-band-edge distribution. The estimated  $\delta_0$  parameter is well consistent with that

obtained from *ab initio* calculations. The present theory also provides a qualitative description of the temperature-activated Hall mobility measured in IGZO at different carrier concentrations. The formulated generalized EMA model goes beyond the traditional multiple trap-and-release (MTR) concept and encompasses both multiple trapping transport and band-type transport dominated regimes in a disordered semiconductor.

## II. THEORETICAL MODEL

We consider an amorphous semiconductor where structural disorder can give rise to potential variations that, in turn, result in the coexistence of randomly distributed localized states and extended states. In the present study we will limit our consideration to a disordered semiconductor with an exponential DOS distribution of localized states that is appropriate for inorganic disordered solids [3] and we focus here on *amorphous oxide semiconductors*. In the present paper we will compare our model with relevant experimental data obtained for a-IGZO films as a representative high-mobility disordered medium. At finite temperature and at large carrier concentration some fraction of the charge carriers are in extended states above the conduction-band edge, which are characterized by a high mobility and contribute to the conductivity, while the others are located in localized states characterized by a very low hopping mobility of charge carriers between them.

A key assumption of our model is that the disorder in a solid can play a dual role—namely, not only generate localized states in the band gap, but also gives rise to random spatial potential variation of the conduction-band edge  $\varepsilon_m$  as schematically illustrated for the two-dimensional case in the inset to Fig. 1. By  $\varepsilon_m$  we actually mean a “local conduction-band edge,” i.e., an energy separating localized and delocalized states. We assume that the spatial potential variations are sufficiently *smooth* with the characteristic length of variations larger than the mean free path of a charge carrier so that the local electrical conductivity can be treated classically, but much

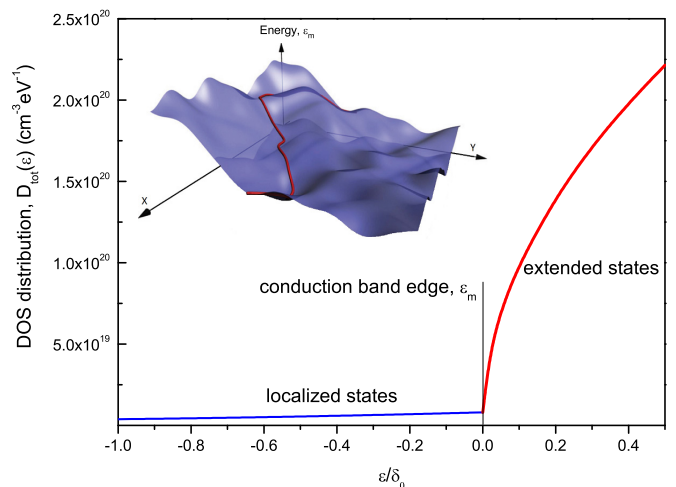


FIG. 1. Cumulative DOS  $D_{\text{tot}}(\varepsilon)$  distribution calculated according to Eq. (6) including localized and delocalized states using parameters  $N_m = 8 \times 10^{18} \text{ cm}^{-3} \text{ eV}^{-1}$ ,  $D_{C0} = 1.4 \times 10^{21} \text{ cm}^{-3} \text{ eV}^{-3/2}$ , and  $E_0 = 0.067 \text{ eV}$  [34]. The inset shows a schematic two-dimensional representation of spatial fluctuation of the band edge  $\varepsilon_m$ .

smaller than the length of the system. The potential variations are considered to be independent of one another.

Generally, it is worth noting that the concept of long-range static potential fluctuations that modulate the conduction-band edge in disordered semiconductors is not new and has been widely applied to heavily doped and highly compensated semiconductors (HDCSs) [22]. Band-edge fluctuations were also invoked to describe electrical conduction in chalcogenide glasses (see Ref. [35] for review) and in solid semiconductor solutions [36]. It has been shown that in analogy with HDCS, the concept of long-range fluctuations is also applicable to amorphous semiconductors [37] and the theories exploiting random potential fluctuations were used to interpret the data for transport phenomena and the optical absorption in doped a-Si:H [38,39]. This concept was often used as an alternative description to the more conventional models of charge-carrier transport in noncrystalline materials based on pointlike band-tail localized states [13,38].

Further we assume that the random long-range variations of  $\varepsilon_m$  are described by a Gaussian distribution with the standard deviation  $\delta_0$

$$g(\varepsilon_m) = \frac{1}{\delta_0 \sqrt{2\pi}} \exp \left[ -\frac{1}{2} \left( \frac{\varepsilon_m}{\delta_0} \right)^2 \right]. \quad (1)$$

It should be noted that a Gaussian-type distribution of potential barriers in disordered inorganic semiconductors was suggested long ago in terms of the Thomas-Fermi approximation [28] and then used in some percolation theories [40]. We have further corroborated this notion by *ab initio* calculations of an amorphous IGZO, which demonstrated that the variation of the conduction-band edge in this material is consistent with Eq. (1) and will be shown further below.

For calculating the charge transport properties, the cumulative (total) density-of-state (DOS) distribution in the whole energy range is needed. The distribution of the localized states at  $\varepsilon < \varepsilon_m$  in inorganic semiconductors normally has an exponential profile with the width  $E_0$ ,

$$D_L(\varepsilon) = N_m \exp \left( \frac{\varepsilon - \varepsilon_m}{E_0} \right), \quad (2)$$

where  $N_m$  is the density of localized states at the band edge. In crystalline materials devoid of disorder and localized states, the density of extended (transport band) states at  $\varepsilon > \varepsilon_m$  is usually approximated as [20]

$$D_C(\varepsilon) = D_{C0} \sqrt{\varepsilon - \varepsilon_m}, \quad (3)$$

where for a-IGZO thin films  $D_{C0} = 1.4 \times 10^{21} \text{ cm}^{-3} \text{ eV}^{-3/2}$  has been reported before [21].

To obtain a total DOS for the system we proceed from the condition that the density of localized states is equal to that of the delocalized states at  $\varepsilon = \varepsilon_m$ ; i.e.,  $D_L(\varepsilon_m) = D_C(\varepsilon_m)$ . Equation (3) can be rewritten as

$$D_C(\varepsilon) = D_{C0} \sqrt{\varepsilon - \varepsilon_m + \Delta}. \quad (4)$$

Equalizing Eqs. (2) and (4) at  $\varepsilon_m$  yields a relation for  $\Delta$ :

$$\Delta = \left( \frac{N_m}{D_{C0}} \right)^2. \quad (5)$$

The total DOS can then be obtained in general form as

$$D_{\text{tot}}(\varepsilon, \varepsilon_m) = \theta(\varepsilon - \varepsilon_m) D_{C0} \sqrt{\varepsilon - \varepsilon_m + \left( \frac{N_m}{D_{C0}} \right)^2} + \theta(\varepsilon_m - \varepsilon) N_m \exp \left[ \frac{\varepsilon - \varepsilon_m}{E_0} \right], \quad (6)$$

where  $\theta(t)$  is the unit function:  $\theta(t) = 1$  if  $t \geq 0$  and  $\theta(t) = 0$  if  $t < 0$ .

The relative weight of localized states with respect to delocalized ones in the cumulative DOS distribution is critically important for quantitative fitting of experimental results in relevant amorphous semiconductors. In Fig. 1 we depict a cumulative DOS  $D_{\text{tot}}(\varepsilon)$  using realistic parameters already reported for a-IGZO films, namely  $N_m = 8 \times 10^{18} \text{ cm}^{-3} \text{ eV}^{-1}$  and  $E_0 = 0.067 \text{ eV}$  from Ref. [34], as appropriate representative values. Although the DOS distribution in Fig. 1 has a discontinuity at  $\varepsilon_m = 0$  we consider it as a sufficiently good approximation for the a-IGZO films.

### III. THEORETICAL RESULTS

#### A. The drift mobility

Let  $\sigma$  be the dc conductivity of the system. The key point of the present calculations is that the *effective* longitudinal drift conductivity  $\sigma_e$  in a disordered system under a weak electric field  $\mathbf{E} = \{E, 0, 0\}$  can be calculated by the effective medium approximation (EMA) method suggested earlier by Kirkpatrick [23] and also verified by our group recently [26], which leads to the following self-consistency equation for  $\sigma_e$ :

$$\left\langle \frac{\sigma(\varepsilon_m) - \sigma_e}{\sigma(\varepsilon_m) + (d-1)\sigma_e} \right\rangle = 0, \quad (7)$$

where  $\sigma(\varepsilon_m)$  is the ‘‘local’’ conductivity at the band edge and  $d$  is the spatial dimension. Hereafter we consider a three-dimensional (3D) system. Angular brackets  $\langle \dots \rangle$  denote the configuration averaging over the distribution of  $\sigma(\varepsilon_m)$ , or more specifically it implies averaging over an ensemble of  $\varepsilon_m$  values at some space point employing the distribution given by Eq. (1). Thus, we in fact use here the ergodic hypothesis which assumes that for an infinite system the spatial average is the same as the statistical ensemble average.

Hereafter we consider a disordered system with the cumulative DOS distribution (Fig. 1) given by Eq. (6) and assume that charge carriers are distributed over the total DOS in the way that some part of them occupy extended states and the rest are in localized states depending on the position of the Fermi level  $\varepsilon_F$ . The total local concentration of charge carriers at a given  $\varepsilon_m$  value can be calculated as

$$n_{\text{tot}}(\varepsilon_m) = D_{C0} \int_{\varepsilon_m}^{\infty} d\varepsilon \frac{\sqrt{\varepsilon - \varepsilon_m + \left( \frac{N_m}{D_{C0}} \right)^2}}{1 + \exp \left( \frac{\varepsilon - \varepsilon_F}{k_B T} \right)} + N_m \int_{-\infty}^{\varepsilon_m} d\varepsilon \frac{\exp \left( \frac{\varepsilon - \varepsilon_m}{E_0} \right)}{1 + \exp \left( \frac{\varepsilon - \varepsilon_F}{k_B T} \right)}. \quad (8)$$

Since the charge-carrier mobility through the extended states is generally much higher than the hopping charge

mobility via the manifold of the localized states, the conductivity is dominated by the charge carriers in extended states above  $\varepsilon_m$ . In the present model we neglect any hopping transitions between localized states. Therefore the local concentration of mobile charge carriers at arbitrary  $\varepsilon_m$  is

$$n(\varepsilon_m) = D_{C0} \int_{\varepsilon_m}^{\infty} d\varepsilon \frac{\sqrt{\varepsilon - \varepsilon_m + \left(\frac{N_m}{D_{C0}}\right)^2}}{1 + \exp\left(\frac{\varepsilon - \varepsilon_F}{k_B T}\right)}. \quad (9)$$

The local drift conductivity  $\sigma(\varepsilon_m)$  at arbitrary  $\varepsilon_m$ , i.e., at a given point of varying  $\varepsilon_m$  potential surface (cf. Fig. 1, inset), can be written as

$$\sigma(\varepsilon_m) = e\mu_0 n(\varepsilon_m), \quad (10)$$

where  $e$  is the elementary charge and

$$\mu_0 = \frac{e}{m^*} \langle \tau \rangle \quad (11)$$

is the intrinsic (band) drift charge-carrier mobility in extended states determined by the electronic effective mass  $m^*$  and the average scattering time  $\langle \tau \rangle$ , which for simplicity's sake is considered as a constant at this stage.

The Fermi level  $\varepsilon_F$  in the system can be calculated using the *total average* concentration  $n_{\text{tot}}$  of charge carriers in the whole system (the average carrier concentration in a semiconductor) from  $n_{\text{tot}} = \int_{-\infty}^{\infty} d\varepsilon D_{\text{tot}}(\varepsilon) \{1 + \exp[(\varepsilon - \varepsilon_F)/k_B T]\}^{-1}$ . The total concentration  $n_{\text{tot}}$  is defined as sum of concentrations of charge carriers in extended states  $n_1$  and in localized states  $n_2$ , which could be calculated by averaging Eq. (8) over the distribution given by Eq. (1),

$$n_{\text{tot}} = n_1 + n_2, \quad (12)$$

where

$$n_1 = \frac{1}{\delta_0 \sqrt{2\pi}} \int_{-\infty}^{\infty} d\varepsilon_m \exp\left[-\frac{1}{2} \left(\frac{\varepsilon_m}{\delta_0}\right)^2\right] \times D_{C0} \int_{\varepsilon_m}^{\infty} d\varepsilon \frac{\sqrt{\varepsilon - \varepsilon_m + \left(\frac{N_m}{D_{C0}}\right)^2}}{1 + \exp\left(\frac{\varepsilon - \varepsilon_F}{k_B T}\right)}, \quad (13)$$

$$n_2 = \frac{1}{\delta_0 \sqrt{2\pi}} \int_{-\infty}^{\infty} d\varepsilon_m \exp\left[-\frac{1}{2} \left(\frac{\varepsilon_m}{\delta_0}\right)^2\right] \times N_m \int_{-\infty}^{\varepsilon_m} d\varepsilon \frac{\exp\left[\frac{\varepsilon - \varepsilon_m}{E_0}\right]}{1 + \exp\left(\frac{\varepsilon - \varepsilon_F}{k_B T}\right)}. \quad (14)$$

Although we assume here that the charge carriers with concentration  $n_2$  in localized states do not contribute to the conductivity, these carriers must, however, be taken into account for the calculation of the Fermi level  $\varepsilon_F$ , it being determined by  $n_{\text{tot}}$ . In fact, the conductivity is determined by the carriers in extended states with concentration  $n_1$ ; therefore, it is effectively  $n_1 = n_e$ .

Substituting Eq. (10) in (7), the subsequent configuration averaging in Eq. (7) yields the following transcendental

equation for the effective drift conductivity  $\sigma_e$ :

$$\int_{-\infty}^{\infty} dt \exp\left(-\frac{1}{2}t^2\right) \frac{\int_t^{\infty} dt_1 \frac{\sqrt{t_1 - t + b}}{1 + \exp[x(t_1 - x_F)]} - X_e}{\int_t^{\infty} dt_1 \frac{\sqrt{t_1 - t + b}}{1 + \exp[x(t_1 - x_F)]} + 2X_e} = 0, \quad (15)$$

where  $X_e = \sigma_e/\sigma_0$ ,  $\sigma_0 = e\mu_0 D_{C0} \delta_0^{3/2}$ ,  $x = \delta_0/k_B T$ ,  $x_F = \varepsilon_F/\delta_0$ , and  $b = (N_m/D_{C0})^2/\delta_0$ . The effective drift mobility in extended states can then be obtained as

$$\mu_e = \sigma_e/en_e, \quad (16)$$

where the effective drift conductivity  $\sigma_e$  is given by Eq. (15).

It should be pointed out that the presented model basically reduces to the well-known multiple trap-and-release (MTR) model in the limiting case devoid of the spatial variations of the conduction-band edge  $\varepsilon_m$  (i.e., at  $\delta_0 \rightarrow 0$ ).

Figure 2(a) (red bold curves) shows the charge-carrier drift mobility  $\mu_e$  as a function of temperature calculated for different charge-carrier concentrations within the present EMA model in a disordered semiconductor with the cumulative DOS given by Eq. (6) and assuming a Gaussian distribution of  $\varepsilon_m$  with standard deviation  $\delta_0 = 0.05$  eV in Eq. (1). The thermally activated character of the charge transport in such system is evident and it is largely determined by the disorder-induced distribution of  $\varepsilon_m$  provided that the density of localized states at the conduction-band edge is rather small, e.g.,  $N_m = 8 \times 10^{18} \text{ cm}^{-3} \text{ eV}^{-1}$  as it is for a-IGZO films [34]. At such material parameters, the localized states *do not alter significantly* the calculated temperature dependences [blue dashed curves in Fig. 2(a)], and can therefore be neglected. Note that when reducing  $\delta_0$  tenfold to 0.005 eV, all curves at considered carrier concentrations collapse into a single, temperature-independent graph [upper bunch of curves in Fig. 2(a)] as expected for a system without potential fluctuations of the conduction-band edge.

The calculated  $\mu_e(T)$  dependences can be well approximated by linear dependences in an Arrhenius representation [thin straight lines in Fig. 2(a)] which, rather, feature a so-called Meyer-Neldel (MN) compensation behavior [25,27]; i.e.,  $\ln(\mu_{FE})$  vs  $T^{-1}$  graphs intersect at some finite isokinetic temperature ( $T_{\text{MN}}$ ) when extrapolated to a higher temperature. The MN compensation phenomenon has often been observed for thin-film field-effect transistor (FET) characteristics, e.g., in amorphous Si, chalcogenide glasses, and amorphous oxides as well as in organic FETs [25,27,41,42]. The results in Fig. 2(a) are closely reminiscent of a MN behavior described recently for the FET charge-carrier mobility in the hopping transport regime within a Gaussian distribution of localized states [25,27].

The temperature-dependent effective conductivities  $\sigma_e(T)$  calculated by Eq. (15) for different carrier concentrations in the same system are shown in Fig. 2(b) (bold red curves). Thin straight lines in Fig. 2(b) depict the asymptotes to the above-calculated Arrhenius plots made in the temperature range where the  $\ln(\sigma_e/\sigma_0) \propto 1/T$  law is obeyed. It is remarkable that the asymptotes to the set of  $\sigma_e(T)$  curves feature a single crossing point at a “negative” temperature [Fig. 2(b)]. This is reminiscent of the so-called inverse-MN rule (or anti-Meyer-Neldel rule) behavior with negative MN energy, that is in contrast to the normal MN-type behavior

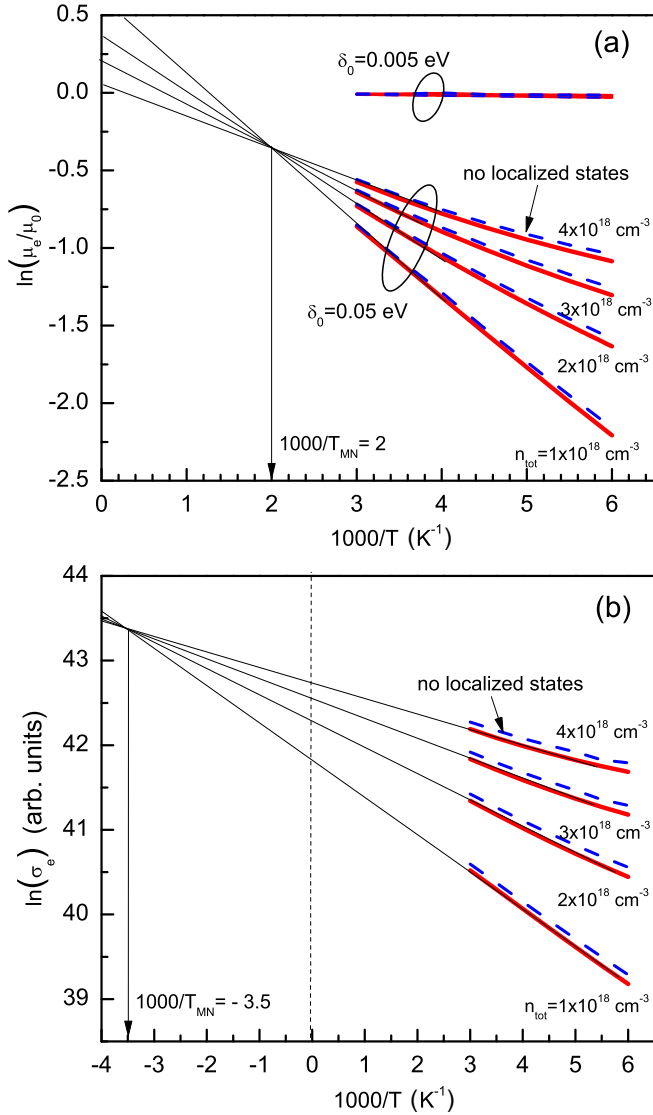


FIG. 2. Temperature dependences of the effective charge-carrier mobility  $\mu_e$  (a) and conductivity  $\sigma_e$  (b) calculated at different carrier concentrations  $n_{tot}$  (red bold curves) in a disordered system with the cumulative DOS given by Eq. (6) using  $N_m = 8 \times 10^{18} \text{ cm}^{-3} \text{ eV}^{-1}$  and  $E_0 = 0.067 \text{ eV}$  from Ref. [34] and assuming  $\delta_0 = 0.05 \text{ eV}$ . Note that the upper bunch of curves in (a) was calculated at much smaller  $\delta_0 = 0.005 \text{ eV}$  and the curves virtually coincide at the considered carrier concentrations. The same calculations were done for a DOS distribution devoid of the localized states and accounting for the extended states only using the same  $\delta_0$  values (blue dashed lines). Thin straight lines represent the approximations toward a higher temperature. The isokinetic temperature is indicated by a vertical arrow (note that it is negative for conductivity and positive for mobility). Vertical dashed line in (b) denotes  $1/T = 0$  and is just a guide to the eye.

for the  $\mu_e(T)$  in the same system [Fig. 2(a)]. It should be mentioned that the inverse-MN effect has been observed before for the temperature-dependent conductivity in heavily doped microcrystalline Si [43,44] and some a-Si:H devices [45].

Figure 3 shows carrier-concentration dependence of the drift charge-carrier mobility [ $\ln(\mu_e/\mu_0)$  vs  $n_{tot}$ ] calculated for different temperatures by the present model (red bold curves).

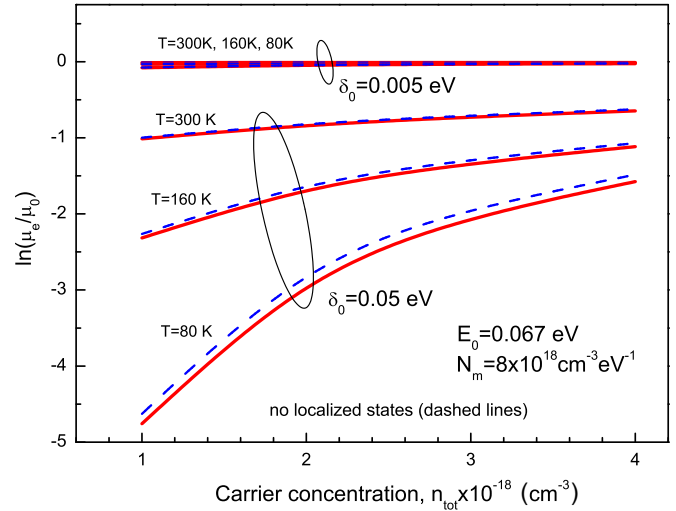


FIG. 3. Dependence of the effective charge-carrier mobility  $\ln(\mu_e/\mu_0)$  on the charge-carrier concentration  $n_{tot}$  at different temperatures calculated within the present model in a disordered system with the DOS distribution given by Eq. (6) assuming  $N_m = 8 \times 10^{18} \text{ cm}^{-3} \text{ eV}^{-1}$ ,  $E_0 = 0.067 \text{ eV}$  [34], and  $\delta_0 = 0.05 \text{ eV}$  (red bold curves). The calculations using  $\delta_0 = 0.005 \text{ eV}$  are shown by the upper bunch of curves. The same carrier-concentration dependences were calculated upon ignoring the localized states and accounting for the extended states only (blue dashed curves).

As expected for a disordered semiconductor, the  $\mu_e$  increases with increasing carrier concentration. This dependence is more pronounced as the temperature decreases. Note that for comparison purposes the upper bunch of curves in Fig. 3 was calculated at much smaller parameter,  $\delta_0 = 0.005 \text{ eV}$ , and the curves virtually were found to coincide at all temperatures featuring no noticeable carrier concentration dependence.

In order to check whether the spatial fluctuations of the  $\varepsilon_m$  [cf. Eq. (1)] or, rather, the localized states, contribute most to the temperature and carrier-concentration dependence of  $\mu_e$  and  $\sigma_e$  in the considered disordered system, we performed calculations using the DOS distribution devoid of the localized states and accounting for the extended states only. The results are presented in Figs. 2 and 3 by dashed blue curves and they suggest that the temperature and carrier-concentration dependences of  $\mu_e$  and  $\sigma_e$  in the considered carrier concentration range are governed mostly by potential variations of the conduction-band edge and are not limited by the localized states, provided that their density is sufficiently small. Localized states might therefore be disregarded in some materials, e.g., in a-IGZO films where the realistic density of localized states at the conduction-band edge is  $N_m = 8 \times 10^{18} \text{ cm}^{-3} \text{ eV}^{-1}$ . Such a behavior seems to be specific to oxide semiconductor films owing to relatively low  $N_m$  in these materials, which is direct cause for the Fermi level to be very close or within the conduction band.

### B. The Hall mobility

To calculate the effective Hall conductivity  $\sigma_e^{xy}$  in the same system we use the EMA approach suggested earlier by Cohen and Jortner [46] for the Hall effect under a weak electric field

in disordered materials:

$$\sigma_e^{xy} = \frac{\left\langle \frac{\sigma^{xy}(\varepsilon_m)}{[\sigma(\varepsilon_m) + (d-1)\sigma_e]^2} \right\rangle}{\left\langle \frac{1}{[\sigma(\varepsilon_m) + (d-1)\sigma_e]^2} \right\rangle}, \quad (17)$$

where  $d$  is the spatial dimension of the system (3D in this study) and angular brackets  $\langle \dots \rangle$  denote here the averaging over the ensemble of  $\varepsilon_m$  values using the distribution given by Eq. (1). Local Hall conductivity  $\sigma^{xy}(\varepsilon_m)$  as function of magnetic field  $\mathbf{H} = \{0, 0, H\}$  is defined as [47]

$$\sigma^{xy}(\varepsilon_m) = e\mu_0^{xy} n(\varepsilon_m) \frac{\mu_0 H}{c}, \quad (18)$$

where  $c$  is the speed of light,  $n(\varepsilon_m)$  is given by Eq. (9), and

$$\mu_0^{xy} = \frac{e}{m^*} \frac{\langle \tau^2 \rangle}{\langle \tau \rangle} \quad (19)$$

is the intrinsic Hall mobility in extended states. Here  $\langle \tau^2 \rangle$  is the average of the square of the scattering time, which for simplicity's sake is considered here as a constant as well.

Substituting Eqs. (10), (15), and (18) in Eq. (17), the subsequent configuration averaging in Eq. (17) yields to the relation for the effective Hall conductivity  $\sigma_e^{xy}$  as

$$X_e^{xy} = \frac{\int_{-\infty}^{\infty} dt \exp\left(-\frac{1}{2}t^2\right) \frac{\int_{-\infty}^{\infty} dt_1 \frac{\sqrt{t_1-t+b}}{1+\exp[x(t_1-xF)]}}{\left\{ \int_{-\infty}^{\infty} dt_1 \frac{\sqrt{t_1-t+b}}{1+\exp[x(t_1-xF)]} + 2X_e \right\}^2}}{\int_{-\infty}^{\infty} dt \exp\left(-\frac{1}{2}t^2\right) \frac{1}{\left\{ \int_{-\infty}^{\infty} dt_1 \frac{\sqrt{t_1-t+b}}{1+\exp[x(t_1-xF)]} + 2X_e \right\}^2}}, \quad (20)$$

where  $X_e^{xy} = \sigma_e^{xy}/\sigma_0^{xy}$  and  $\sigma_0^{xy} = e\mu_0^{xy} D_{C0}\delta_0^{3/2}(\mu_0 H/c)$ .

The effective Hall mobility,  $\mu_e^{xy} = (c/H)(\sigma_e^{xy}/\sigma_e)$ , takes the form

$$\mu_e^{xy} = F_0^H \mu_0 \frac{X_e^{xy}}{X_e}, \quad (21)$$

where  $F_0^H = \langle \tau^2 \rangle / \langle \tau \rangle^2$  is the Hall factor, i.e., the ratio of the intrinsic Hall mobility to the intrinsic drift mobility  $\mu_0^{xy}/\mu_0$ . The ratio between *effective* Hall and drift mobilities  $\mu_e^{xy}/\mu_e$  is then determined as

$$\frac{\mu_e^{xy}}{\mu_e} = F_0^H \frac{n_e}{D_{C0}\delta_0^{3/2}} \frac{X_e^{xy}}{X_e^2}. \quad (22)$$

The effective Hall concentration,  $n_e^{xy} = 1/eR_e^{xy}$ , is expressed by the Hall coefficient  $R_e^{xy}$ , which is

$$R_e^{xy} = (c/H)(\sigma_e^{xy}/\sigma_e^2) \quad (23)$$

and can be obtained as

$$n_e^{xy} = \frac{D_{C0}\delta_0^{3/2}}{F_0^H} \frac{X_e^2}{X_e^{xy}}. \quad (24)$$

The  $n_e^{xy}/n_e$  ratio between the effective Hall concentration and effective concentrations of charge-carriers in extended states  $n_e$  can be obtained as

$$\frac{n_e^{xy}}{n_e} = \frac{D_{C0}\delta_0^{3/2}}{F_0^H n_e} \frac{X_e^2}{X_e^{xy}}. \quad (25)$$

From Eqs. (22) and (25) it follows that

$$\frac{\mu_e^{xy}}{\mu_e} = \frac{n_e}{n_e^{xy}}. \quad (26)$$

This relation coincides with the classical relation between Hall and drift mobilities in the band transport regime. Note that it was proven to be valid also for materials with some disorder provided that the charge coherence in delocalized states is sufficiently large in the system [48].

Figure 4(a) shows temperature-dependent effective Hall and drift mobilities vs  $\delta_0/k_B T$  calculated within the present model (bold red curves) at different total carrier concentrations in a disordered semiconductor with the cumulative DOS distribution presented in Fig. 1. The material parameters were the same as those used in Figs. 2 and 3. These results clearly reveal a thermally activated behavior of the Hall mobility in the considered disordered system, qualitatively similar to that obtained for the drift charge-carrier mobility. Thin lines represent the approximations toward a higher temperature and the MN-type compensation behavior clearly emerges for both the Hall and drift mobilities. We should note that the obtained  $T_{MN}$  value depends on  $\delta_0$ . However, determining its exact functional dependence is not trivial and requires further investigations. Further, the Hall concentrations calculated by Eq. (25) as function of temperature at different total carrier concentrations  $n_{tot}$  are presented in Fig. 4(b) (bold red curves). Interestingly, the present model predicts that the Hall concentration with respect to the effective concentration of charge carriers in extended states  $n_e^{xy}/n_e$  decreases with decreasing temperature and this effect is more pronounced as  $n_{tot}$  is lower. Approximations of the Arrhenius plots toward a higher temperature are shown by straight thin lines in Fig. 4(b).

Figure 5(a) shows the ratio between effective Hall mobilities and drift mobilities  $\mu_e^{xy}/\mu_e$  (red curve) and the ratio between the concentration of charge carriers that contribute to the Hall effect and the concentration of charge carriers in extended states (blue curve)  $n_e^{xy}/n_e$  calculated for a disordered semiconductor with a cumulative DOS distribution given by Eq. (6) at different temperatures. Figure 5(b) shows the same calculations done at room temperature yet for different  $\delta_0$  parameters. The calculated drift mobility  $\mu_e/\mu_0$  as function of  $\delta_0$  is also shown in Fig. 5(b) (green line).

### C. Computation of the electronic structure of a-IGZO

To provide deeper insights into the electronic structure and the properties of the conduction band of amorphous IGZO, we carried out first-principles calculations in the framework of the plane wave density functional theory (DFT) and ultrasoft pseudopotentials [49], as implemented in QUANTUM ESPRESSO [50]. We used the Perdew-Burke-Ernzerhof [51] exchange-correlation density functional combined with a Hubbard correction term of  $U = 6.08$  eV to account for the electron correlation effects on the electronic structure and on the band gap. A set of 16 different amorphous InGaZnO<sub>4</sub> models has been generated, each constituted of a unit cell of 105 atoms of InGaZnO<sub>4</sub>. The structures were generated using classical molecular dynamics with the LAMMPS software [52], following a melt and quenching technique [53] and the parametrization of

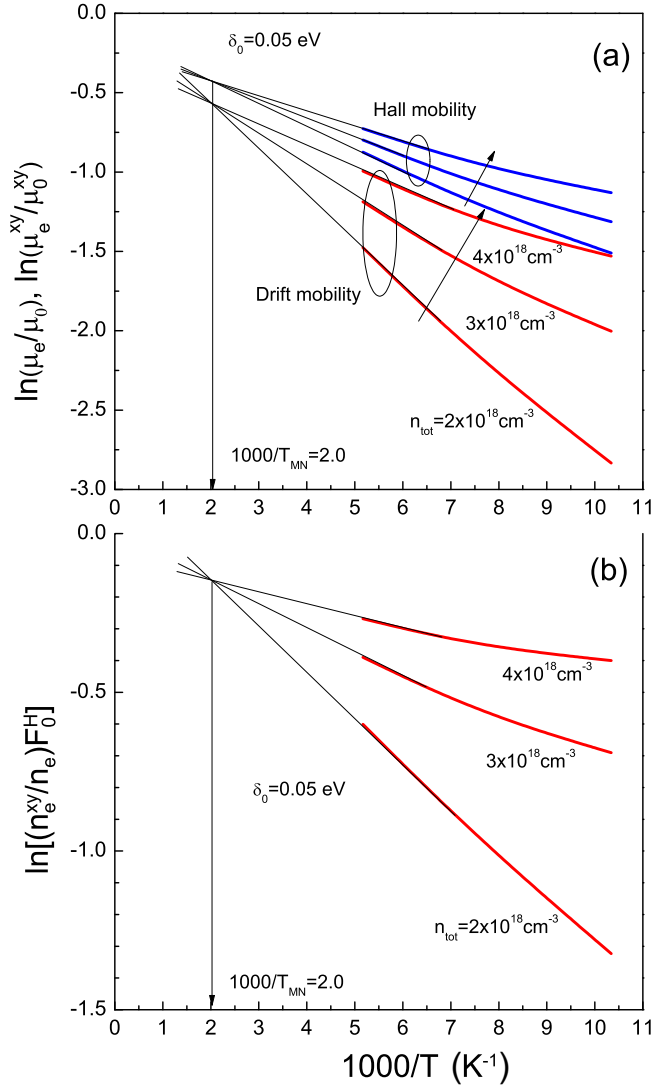


FIG. 4. (a) Comparison of temperature dependences of the Hall mobility  $\ln(\mu_e^{xy}/\mu_0^{xy})$  and effective drift charge-carrier mobility calculated by Eqs. (21) and (16), respectively, assuming  $\delta_0 = 0.05 \text{ eV}$  (bold curves) at different total carrier concentrations  $n_{\text{tot}}$  in a disordered system with the cumulative DOS distribution given by Eq. (6) at  $N_m = 8 \times 10^{18} \text{ cm}^{-3} \text{ eV}^{-1}$ ,  $E_0 = 0.067 \text{ eV}$  [34]. (b) Arrhenius plots of temperature-dependent Hall concentrations normalized to the effective concentration of charge carriers in extended states,  $n_e^{xy}/n_e$  vs  $\delta_0/k_B T$ , calculated by Eq. (24) for different concentrations  $n_{\text{tot}}$ . Thin lines in (a) and (b) represent the approximations toward a higher temperature.  $F_0^H = \langle \tau^2 \rangle / \langle \tau \rangle^2$  is the Hall factor. The isokinetic temperature is indicated by a vertical arrow.

the Buckingham potential proposed by Orita *et al.* [54]. Those amorphous structures were then relaxed in DFT. The detailed characterization and study of these structures is reported in [55].

As already shown by Hosono *et al.* [2,29,56], the conduction band in all the models of a-IGZO is delocalized and should allow a band conduction mechanism. This delocalization in the conduction band can be observed in the pseudo-band-structure given in Fig. 6(a). In opposition, the valence states have a mostly localized character. It is worth mentioning that

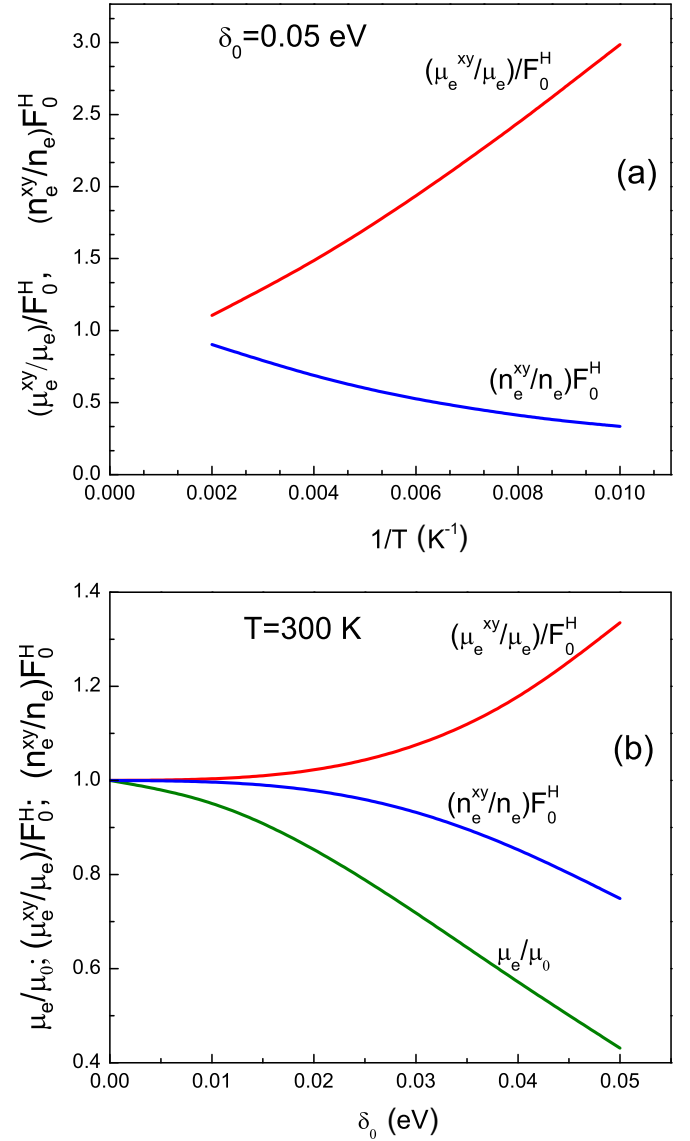


FIG. 5. Ratio between effective Hall and drift mobilities  $\mu_e^{xy}/\mu_e$  (red curve) and the ratio between the effective concentrations of charge carriers that contribute to the Hall effect and charge carriers in extended states  $n_e^{xy}/n_e$  (blue curve) calculated by Eqs. (22) and (24) using  $N_m = 8 \times 10^{18} \text{ cm}^{-3} \text{ eV}^{-1}$ ,  $n_{\text{tot}} = 2 \times 10^{18} \text{ cm}^{-3}$  and  $E_0 = 0.067 \text{ eV}$  from Ref. [34] for a disordered semiconductor assuming  $\delta_0 = 0.05 \text{ eV}$  at different temperatures (a) and at different disorder parameter  $\delta_0$  at  $T = 300 \text{ K}$  (b). Lower green line in (b) shows the effective drift mobility  $\mu_e/\mu_0$  calculated as function of  $\delta_0$ .  $F_0^H = \langle \tau^2 \rangle / \langle \tau \rangle^2$  is the Hall factor.

the pseudo-band-structure arises from the periodic boundary conditions used in the first-principles calculation for the amorphous structures. They are therefore structure specific in contrast to normal crystalline band structures. Our calculations within this approach yield an effective mass of  $0.28m_e$ , which is in good agreement with the reported experimental values of  $0.34m_e$  [57] and  $0.36m_e$  [58]. This matching confirms the validity of our approach. We found a similar isotropic value of  $m^* = 0.28 m_e$  in the crystalline phase of IGZO [55], which suggests that the impact of the amorphization on the electron

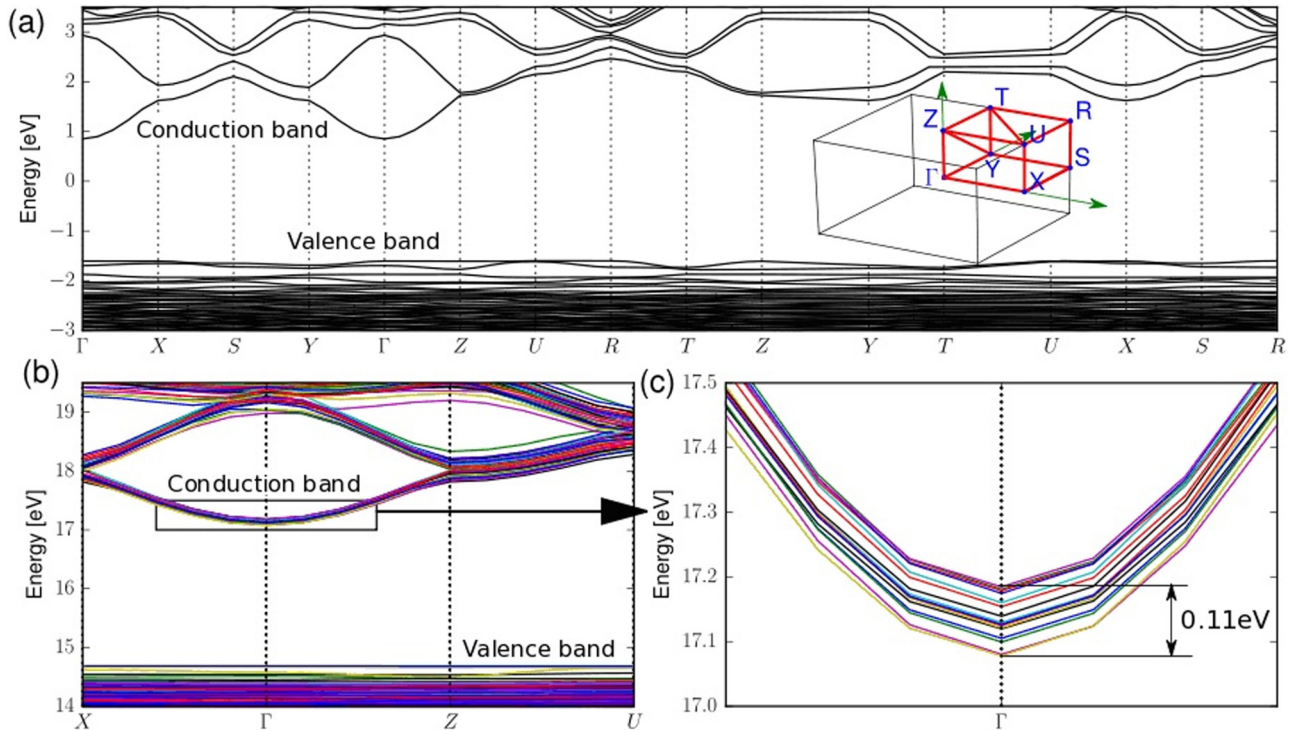


FIG. 6. (a) Pseudo-band-structure of an amorphous IGZO structure. The inset shows the  $k$ -point set used to sample the first Brillouin zone. The zero of energy is set at the Fermi energy. In spite of the amorphous structure, the conduction band remains delocalized in all the 16 amorphous structures due to the contribution of the  $s$  orbitals of the cations. (b) Cumulative plot of the pseudo-band-structure of the 16 amorphous structures obtained after alignment on the electronic signature of the deep  $d$  electron of Ga and In (where the zero of energy is set). All the structures have similar dispersion but the bottom of the conduction band is found to vary. (c) Closeup of the bottom of the conduction band. The maximum energy difference between 16 amorphous structures used here is 0.11 eV; Gaussian approximation yields a standard deviation of 0.03 eV for the conduction-band variation.

effective mass of the conduction band is negligible. These calculations also suggest that the amorphization process does not create localized tail states below the conduction band. The latter might be due to defects/impurities in the material. This justifies a quite low density of the localized states for electrons in a-IGZO films [34], which was employed in our EMA charge transport calculations. Thus, in contrast to the pseudo-band-structure of most of the amorphous materials which displays localized conduction bands, our first-principles calculations suggest that the conduction band in a-IGZO is unusually delocalized.

Among the different amorphous structures used, the absolute position of the conduction band is found to be dependent on the model, even after a proper alignment of the electronic structure using the electronic signature of the deep  $d$  electrons of Ga and In is guaranteed. The observed variation is depicted in Figs. 6(b) and 6(c) and is found to be consistent with the model proposed above, even though the number of tested amorphous structures was finite (16). Indeed, the maximum variation observed in the position of the conduction bands was found to be 0.11 eV [cf. Fig. 6(c)], with a standard deviation of 0.03 eV, which is close to  $\delta_0 = 0.04$  eV used for the experimental data fitting shown further below. This variation can be explained by the variations in the metal coordination in the different amorphous structures. An alteration of the coordination modifies locally the interaction between the metal and the oxygen ions. The simulations reveal that

this interaction has a main antibonding character in the conduction band [55]. Therefore, all changes leading to a reduction of this interaction will lessen the conduction-band energy and, thereby, lead to a downward shift. This change in interaction also explains the origin of the difference in the band gap of the crystalline and amorphous phases of IGZO, which is found to be mostly due to a downward shift of the conduction band [55,59]. The latter shift is nevertheless emphasized in this case, since the reduction of the metal coordination between the crystalline and amorphous phase is more pronounced than the variations observed between the different models of the amorphous phase.

#### IV. COMPARISON WITH EXPERIMENT

To verify applicability of the present model, we compare it with experimental results obtained for a-IGZO films that feature both a comparatively large charge-carrier mobility and Hall effect for a disordered material. Temperature- and carrier-concentration-dependent drift mobility and conductivity were studied in FET configuration. The high-performance bottom-gate top-contacts a-IGZO thin-film transistors were fabricated on a highly doped silicon wafer acting as the substrate and the gate electrode. On top of this substrate, a gate-insulating 120-nm-thick layer of silicon dioxide ( $\text{SiO}_2$ ) has been grown by thermal oxidation. The a-IGZO as an  $n$ -channel active layer was deposited using the dc-sputtering technique and

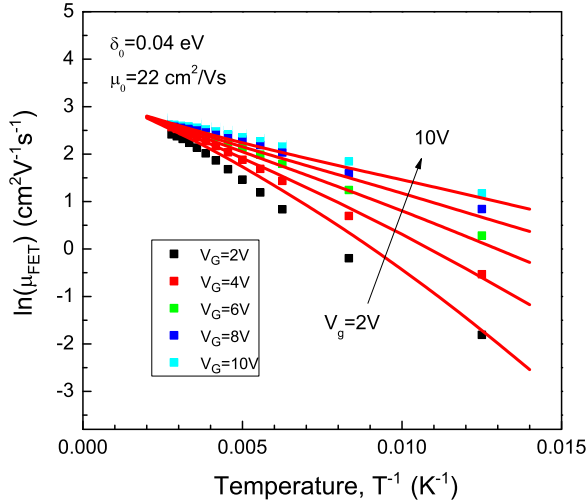


FIG. 7. Arrhenius temperature dependence of the FET mobility  $\mu_{\text{FET}}(T)$  measured in an a-IGZO TFT at different  $V_G$  (symbols) and results of their fitting with Eqs. (15) and (16) (solid lines). Localized states were ignored. Fitting parameters are shown as indicated in the inset.

patterned by wet etching. The details of a-IGZO deposition were described before [60]. Finally, molybdenum source and drain contacts were formed by the lift-off technique. The channel length and width were  $L = 20 \mu\text{m}$  and  $W = 200 \mu\text{m}$ , respectively. The FETs were passivated with a 100-nm-thick  $\text{SiO}_2$  layer using a plasma enhanced chemical vapor deposition (PECVD) chamber and then annealed at  $165^\circ\text{C}$  in  $\text{N}_2$  for 1 h. All layers were patterned using standard photolithography. The transistor characteristics were measured using an Agilent 4156 parameter analyzer in dark under vacuum conditions. For temperature-dependent measurements, the FET device was mounted on the sample holder of a variable temperature “cold-finger” cryostat and characterized in vacuum in the temperature range from 80 to 325 K. The FET mobility has been determined in the linear regime of the  $I_D - V_G$  characteristics at low source-drain voltages  $V_{DS} = 0.1 \text{ V}$ , where  $I_D$  and  $V_G$  is source-drain current and gate voltage, respectively. The fabricated FETs have exhibited state-of-the-art performance characteristics for a-IGZO films with a mobility of  $\mu_{\text{FET}} = 17 \text{ cm}^2/\text{Vs}$ , a subthreshold slope of 0.25 V/decade, an on-off ratio of  $>10^6$ , no hysteresis, and a small threshold voltage ( $V_{th}$ ). Contact resistance of our FETs was found to be negligible at all temperatures, as verified by output characteristics, due to near-Ohmic contacts between IGZO and molybdenum electrodes.

Figure 7 presents the field-effect mobility  $\mu_{\text{FET}}$  (symbols) as a function of inverse temperature measured in an a-IGZO TFT parametric in gate voltages  $V_G$  and fitted by the present model (solid lines). The activation behavior for the  $\mu_{\text{FET}}(T)$  is evident in this material.

We should note that in order to minimize the number of fitting parameters in Fig. 7 the localized states were neglected here. The latter can be justified for the representative material parameters of a-IGZO films [34] and sufficiently large carrier concentrations, as it has been proven by Fig. 2. In fact, the only key fitting parameter in Fig. 7 was  $\delta_0 = 0.04 \text{ eV}$ , while

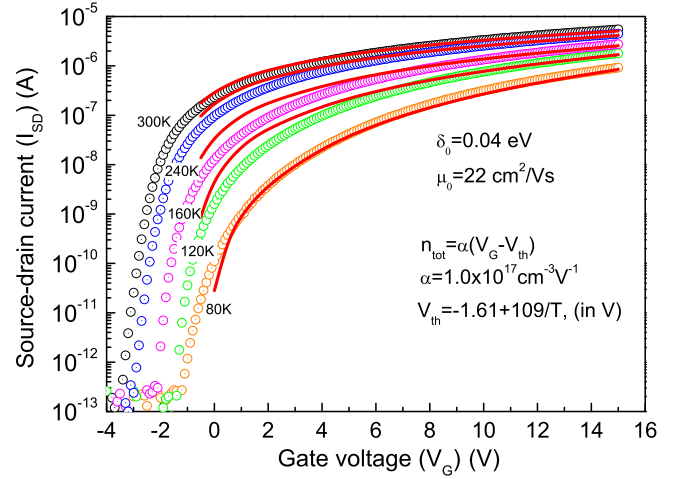


FIG. 8. Transfer characteristics ( $I_{SD}$  vs  $V_G$ ) of a-IGZO TFT measured (symbols) at different temperatures ranging from 80 to 300 K and fitted with the present model for the temperature-dependent conductivity by Eq. (15) ignoring localized states (solid lines). The parameters used in the calculations were the same as in Fig. 7.

the carrier concentration was calculated as a linear function of  $(V_G - V_{th})$  taking into account the observed shift of  $V_{th}$  with temperature. The estimated total carrier concentrations were found to change within  $2.24 \times 10^{17} < n_{\text{tot}} < 1.32 \times 10^{18} \text{ cm}^{-3}$  when the gate voltage was ranging within  $V_G = 2 - 12 \text{ V}$  at  $80 < T < 300 \text{ K}$ . To keep this paper focused, we limit our consideration to the  $\mu_0 = \text{const.}$  approximation [cf. Eq. (11)] which does not significantly alter the results in the focus of the present study. The intrinsic mobility  $\mu_0$  is obtained by fitting the experimental data of a-IGZO with the present model and this yields  $\mu_0 = 22 \text{ cm}^2/\text{Vs}$ . It worth noting that this value is not much different from the *intrinsic* (band) mobility  $\mu_0$  in a-Si:H determined by extrapolating experimental electron drift mobility data to infinite temperature (see, for review, Ref. [61]); therefore it cannot be a cause of very different *effective* mobility values observed in FET devices based on a-IGZO and a-Si:H.

Figure 8 shows transfer characteristics ( $I_{SD}$  vs  $V_G$ ) measured in the a-IGZO TFT at different temperatures (symbols) and fitted by the present model by Eq. (15) (solid lines) in above-threshold voltage region. It should be noted that these fitting  $I_{SD}(T)$  curves were in fact used to get theoretical  $\mu_e(T)$  dependences presented in Fig. 7 (solid curves) by differentiating  $\mu_e \propto dI_{SD}/dV_G$ . This corresponds to the theoretical relation  $\mu_e = (1/e)d\sigma_e/dn$ . A reasonably good agreement between experimental data and the present EMA model can be seen in Figs. 7 and 8, implying that despite the above simplifications the present model reproduces adequately basic features of the temperature-activated and carrier-concentration-dependent charge transport in a-IGZO films. Note that the threshold voltage  $V_{th}$  in this a-IGZO TFT is slightly shifted to a negative voltage. This is known to be due to intrinsic doping of a-IGZO film implying that the observed conductivity at  $V_G \leq 0$  is not due to formation of the conductive channel but rather is due to a bulk conductivity in the film.

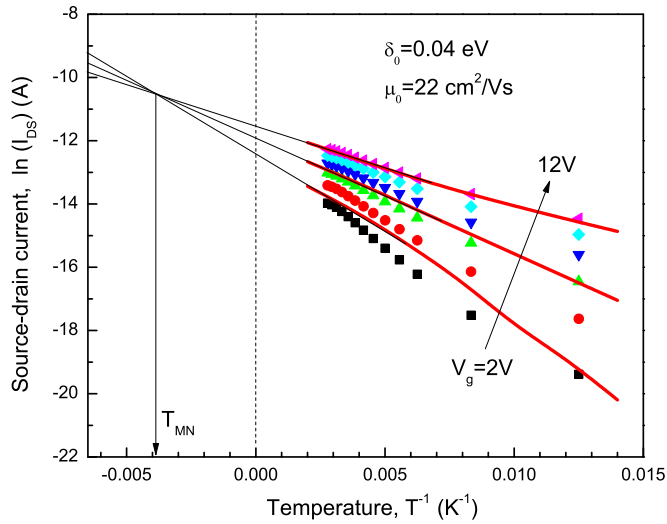


FIG. 9. Source-drain current ( $I_{SD}$ ) vs  $1/T$  measured in a-IGZO TFT at different gate voltages  $V_G$  (symbols) and fitted with Eq. (15) for the conductivity (bold red lines). Thin straight lines represent the approximations toward a higher temperature. The isokinetic temperature is indicated by a vertical arrow (note that it is negative). Vertical dashed line at  $T^{-1} = 0$  is just a guide to the eye.

Figure 9 shows Arrhenius plots of temperature-dependent source-drain current ( $I_{SD}$ ) measured at different gate voltages in a-IGZO films in TFT geometry in the above-threshold voltage region (symbols). We assume here that the current density is proportional to the conductivity as the source-drain voltage was the same in these measurements. Fitting of the experimental  $I_{SD}(T)$  data in Fig. 9 was done by Eq. (15), ignoring localized states as mentioned above which can be justified for this material at sufficiently large  $V_G$ , as documented by the good agreement between experiment and theory (see solid curves in Fig. 9). It is evident that the extrapolations of these graphs intersect at a *negative* isokinetic temperature featuring the *inverse-MN* compensation effect for the conductivity, which perfectly agrees with prediction of the present theory for such an amorphous system [cf. Fig. 2(b)]. It should be mentioned that a similar inverse-MN effect has been already reported for  $I_{SD}(T)$  data in a-IGZO TFT measured in the above-threshold voltage region [62]. It is in sharp contrast to the mobility data presented in Fig. 7 obtained for the same a-IGZO TFT, which shows “normal” MN-type behavior well predicted by the present model. Thus, both sets of experimental data in Figs. 7 and 9 can be fitted by the present model using the same parameters.

To compare the present model with experimental results on the Hall effect in a-IGZO films, we fitted Hall mobilities reported before by Kamiya *et al.* [33] for different temperatures and different carrier concentrations created by deliberate doping in a-IGZO films shown by symbols in Fig. 10(a). The Hall mobilities calculated within the present model are shown by solid lines. Figure 10(b) shows temperature dependences of the drift conductivity measured in the same a-IGZO films and the calculations by the present model (solid lines). We should note that both drift conductivity and Hall mobility were calculated using the same  $\delta_0 = 0.04$  eV as the only fitting parameter. Neither scattering effects on

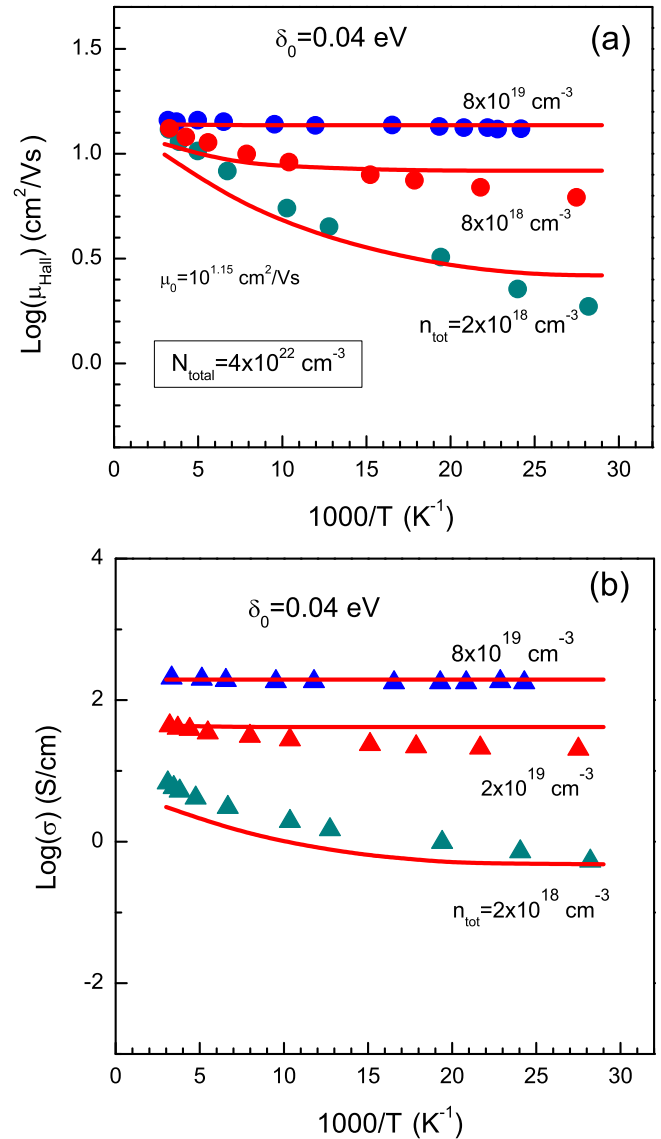


FIG. 10. (a) Temperature dependence of the Hall mobility in a-IGZO films (experimental data from Ref. [33]) measured at different carrier concentrations created by deliberate doping (symbols) and results of their fitting by the present model (solid lines). Carrier concentrations were taken from the experiment. (b) Temperature dependences of the drift conductivity measured in the same a-IGZO films [33] and results of their fitting by the present model (solid lines).

the intrinsic charge transport nor localized states were taken into account. Despite such simplifications, the present model describes the experimental temperature dependences over a broad range from room temperature down to 80 K and reproduces the relative decrease in the Hall mobility and drift conductivity upon lowering the carrier concentration in a satisfactory way. This demonstrates that the present model can provide an adequate basis for a quantitative description of the temperature-activated drift and Hall charge-carrier mobilities in amorphous oxide semiconductors in the large-carrier-concentration transport regime that can be realized by either doping or carrier accumulation in the conductive channel of a FET.

## V. DISCUSSION AND CONCLUSIONS

As described above, the charge transport in high-mobility disordered semiconductors can occur in the regime with a significant degree of degeneration realized at large carrier concentrations when the Fermi level is very close to the transport-band edge. This might be a consequence of both a reduced energy disorder resulting in low density of localized states in the band gap and an enhanced electronic coupling. The degeneration regime cannot probably be reached in strongly disordered materials like a-Si:H or many other conventional disordered (organic and inorganic) semiconductors at realistic carrier concentrations achievable in TFT devices since the density of the localized states is too large. However, it apparently is realized in amorphous oxide semiconductors like a-IGZO and perhaps in some organic TFTs where the FET mobility appears to be relatively high and where, at sufficiently large gate voltages, it features rather small activation energy within a few  $kT$  at room temperature. This means that a large part of the charge carriers (if not a major part in some materials) are in extended states above the conduction-band edge as described by Fermi-Dirac statistics. The latter is a precondition for observation of an ideal Hall effect (i.e.,  $\mu_e = \mu_{\text{Hall}}$ ) implying that the charge carriers contributing to the current are delocalized and move via a predominantly trap-free bandlike mechanism.

It is worth noting that the Hall mobility (and transverse conductivity) in low-mobility disordered systems with hopping transport is normally strongly suppressed because it is determined by three-site (or more) hopping probabilities instead of the two-site probabilities for the drift mobility, that was demonstrated long ago by Böttger and Bryksin [63], Friedman and Pollak [64] for nonpolaronic charge carriers, and also by Emin [65] within the Holstein polaron hopping model. The three-site approximation can give rise to the same sign of the Hall effect for both electrons and holes implying a “sign reversal” effect. Accounting for a larger number of site probabilities can also result in a *double sign reversal* in the Hall effect [66]. Thus, in contrast to crystals, the sign of the Hall effect turns out to be often problematic in disordered systems with hopping charge transport and hence the Hall effect measurements cannot be applied in many instances to determine the sign of the mobile carriers in such systems as, for instance, in doped a-Si:H [67]. Since in the present work we consider a disordered system with very low density of the localized states and with transport through the delocalized states, where the drift charge mobility is scarcely affected by the localized states, the latter are expected to have even lesser impact on the Hall mobility. Therefore the sign reversal and double sign reversal issue is not expected in this case. Within our continual model for a disordered system with free-electron-like Hall effect, the sign of the Hall effect coincides with the sign of movable charge carriers similarly as in crystals (no sign-inversion effect), while it still features some transport properties peculiar to hopping transport systems.

The puzzling thing is that the Hall mobility in a-IGZO is large yet it is associated with a positive activation energy that cannot be rationalized by classical band transport motion. This calls for an extension of the MTR (hopping) theory applied to

disordered semiconductors. The concept of disorder-induced static variation in the transport band of imperfect semiconductors was suggested long ago [28] and can be very useful to formulate a more adequate charge transport model and solve the above puzzle. A similar concept was recently used in the band transport percolation Kamiya-Nomura model [21] to describe the Hall mobility in highly doped a-IGZO films. It assumes a Gaussian-type distribution of potential barriers above the band edge, which has some energy onset in the form  $g(\varepsilon) = \exp[-(\varepsilon - \phi_0)^2/(2\sigma_\phi^2)]$ , where  $\phi_0$ , the average barrier height, and  $\sigma_\phi$ , the energy distribution width, are the major fitting parameters of the model [21,33]. This function differs from the Gaussian distribution originally suggested in Ref. [28] and from Eq. (1) used in the present paper. Apart from the fact that the Kamiya-Nomura model is based on an insufficiently justified calculation method as was already mentioned in the Introduction, this model was never applied to the FET charge-carrier mobilities where carrier concentration in the conductive channel is determined by the gate voltage, but only to the bulk films where carriers were created by doping with electron donors. To describe qualitatively the temperature and carrier-concentration-dependent mobility in doped IGZO films, the authors had to assume that parameters  $\phi_0$  and  $\sigma_\phi$  are changing with changing carrier concentration [21,33], i.e., donor concentration in the a-IGZO film. Thus, these parameters were treated in this model as not material specific but rather operational parameters fitted for each particular carrier concentration used. The fact that the energetic structure of the material changes with carrier concentration is definitely not acceptable for describing the FET mobility and this model is not applicable to pristine (nondoped) a-IGZO films.

The EMA model proposed in the present work is more general since it is not limited to Boltzmann statistics only and based on specific averaging of the Fermi-Dirac carrier distributions using suitably normalized cumulative DOS of superposed extended and localized states distributions. The key assumption of the model is that, in addition to the tail of localized states, the disorder can give rise to spatial energy variation of the transport-band edge being described by a Gaussian distribution with the standard deviation  $\delta_0$  [Eq. (1)] and that the charge carriers move through delocalized states. The presented *ab initio* calculations have perfectly confirmed that the spatial variation of the conduction-band edge really occurs in pristine a-IGZO films as a result of its amorphism while it does not seem to create localized states; the latter are likely originated from some sort of defects in this material. In spite of the amorphous structure, the conduction band in this  $n$ -type semiconductor was found to be basically delocalized, whereas the valence band states have a localized nature (Fig. 6). In the particular case of high-quality a-IGZO TFTs used here, the density of localized states is so low that they can be neglected at large carrier concentrations. It is a general belief that the density of localized states at the conduction-band edge in a-IGZO films is exceptionally low as compared to other disordered semiconductors like a-Si:H, and in our calculations we used the value  $N_m = 8 \times 10^{18} \text{ cm}^{-3} \text{ eV}^{-1}$  reported in a-IGZO with a comparable charge mobility value [34]. It should be mentioned that this conclusion is in variance to the recent finding that the variable range hopping regime is very

relevant to a-IGZO films and its contribution to the overall charge transport is larger than that of the bandlike transport above the conduction-band edge [68]. The discrepancy can probably be explained by a considerably larger density of localized states in a-IGZO films fabricated in Ref. [68] that is also evidenced by much lower charge-carrier mobility in their films.

The principal advantages of the EMA model are that it can describe universally effective drift and Hall mobility in heterogeneous high-mobility materials as a function of disorder, temperature, and carrier concentration within the same theoretical formalism, and can rationalize their thermally activated character. The model predicts that the ratio between effective Hall and drift mobilities  $\mu_e^{xy}/\mu_e$  deviates from unity in a disordered material and the ratio progressively increases with increasing energy disorder parameter  $\delta_0$  and lowering temperature (Fig. 5). To verify the present model we measured the charge-carrier mobility and conductivity in a high-performance a-IGZO TFT at different temperatures and gate voltages. The experimentally obtained  $\sigma_e(T)$  and  $\mu_e(T)$  dependences in the above-threshold voltage region can be described quantitatively in the framework of the present model. Interestingly, that even restricting our consideration solely by the variation of  $\varepsilon_m$ , the EMA model still reproduces reasonably well the basic features of temperature and carrier-concentration-dependent transport measured in our a-IGZO TFTs (cf. Figs. 7–9) using a single fitting parameter  $\delta_0 = 0.04$  eV which is closer to the standard deviation parameter 0.03 eV estimated from results of *ab initio* calculations. At much smaller  $\delta_0 = 0.005$  eV the above effects vanish [see upper branch of curves in Figs. 2(a) and 3]. Within the same theoretical formalism we were able to reproduce also the temperature-dependent Hall mobilities measured in doped a-IGZO films at different carrier concentrations (cf. Fig. 10) using the same  $\delta_0 = 0.04$  eV parameter, that implies that variation of the conduction-band edge might not be much affected by doping of the films.

Another important result of the present study is that the suggested EMA model can reproduce well the Meyer-Neldel type of compensation behavior in degenerate regime [see Fig. 2(a)] regarding the temperature dependences of the charge-carrier mobility upon varying the carrier concentration (gate voltage), which is commonly observed in different TFT devices. Remarkably, the model predicts *distinctly different* MN behavior regarding temperature-dependent charge-carrier mobility and conductivity measured in the same TFT device, namely, an inverse-MN rule for the set of  $\sigma_e(T)$  dependences with isokinetic temperature  $T_{MN}$  at “negative” temperature [Fig. 2(b)] and “normal” MN-type behavior for the  $\mu_e(T)$  dependences with positive  $T_{MN}$  [Fig. 2(a)]. This prediction has been fully supported by experimental results obtained in our high-quality a-IGZO films [cf. Figs. 7 and (9)]. We found that a distinctly different isokinetic temperature  $T_{MN}$  is inherent for the compensation behavior of  $\mu_e(T)$  and  $\sigma_e(T)$  measured in the degenerate regime provided that the charge transport is dominated by Gaussian distribution of the conduction-band-edge variation. Interestingly, a similar phenomenon—positive and negative  $T_{MN}$  temperatures appearing for  $\mu_e(T)$  and  $\sigma_e(T)$  dependences, respectively—was recently predicted by EMA calculations for the hopping transport systems with Gaussian DOS distribution of localized states and verified experimentally in a disordered organic solid [27]. Most probably this phenomenon appears as a consequence of Gaussian-type distribution used to describe these quite different charge transport mechanisms.

#### ACKNOWLEDGMENTS

The research was supported by the European Research Council under the European Union’s Seventh Framework Program (FP7/2007–2013)/ERC Grant Agreement No. 320680 (EPOS CRYSTALLI) and by Volkswagen Foundation (Grant No. 90486).

- 
- [1] *Flexible Electronics: Materials and Applications*, edited by W. S. Wong and A. Salleo, Electronic Materials: Science and Technology (Springer Science+Business Media, New York, 2009).
  - [2] K. Nomura, H. Ohta, A. Takagi, T. Kamiya, M. Hirano, and H. Hosono, *Nature* **432**, 488 (2004).
  - [3] S. Baranovski and O. Rubel, in *Charge Transport in Disordered Solids with Applications in Electronics*, edited by Sergei Baranovski (John Wiley and Sons, Ltd., Chichester, UK, 2006).
  - [4] V. Coropceanu, J. Cornil, D. A. da Silva Filho, Y. Olivier, R. Silbey, and J. L. Brédas, *Chem. Rev.* **107**, 926 (2007).
  - [5] H. Bässler, *Phys. Status Solidi B* **175**, 15 (1993), and references therein.
  - [6] H. Bässler and A. Köhler, *Top. Curr. Chem.* **312**, 1 (2012).
  - [7] D. H. Dunlap, P. E. Parris, and V. M. Kenkre, *Phys. Rev. Lett.* **77**, 542 (1996).
  - [8] Z. G. Yu, D. L. Smith, A. Saxena, R. L. Martin, and A. R. Bishop, *Phys. Rev. Lett.* **84**, 721 (2000).
  - [9] S. D. Baranovskii, I. P. Zvyagin, H. Cordes, S. Yamasaki, and P. Thomas, *Phys. Status Solidi B* **230**, 281 (2002).
  - [10] R. Coehoorn, W. F. Pasveer, P. A. Bobbert, and M. A. J. Michels, *Phys. Rev. B* **72**, 155206 (2005).
  - [11] W. F. Pasveer, J. Cottaar, C. Tanase, R. Coehoorn, P. A. Bobbert, P. W. M. Blom, D. M. de Leeuw, and M. A. J. Michels, *Phys. Rev. Lett.* **94**, 206601 (2005).
  - [12] I. I. Fishchuk, V. I. Arkhipov, A. Kadashchuk, P. Heremans, and H. Bässler, *Phys. Rev. B* **76**, 045210 (2007).
  - [13] H. Overhof and P. Thomas, *Electronic Transport in Hydrogenated Amorphous Semiconductors* (Springer, Heidelberg, 1989).
  - [14] S. D. Brotherton, Transparent amorphous oxide semiconductor TFTs, in *Introduction to Thin Film Transistors* (Springer International Publishing, Cham, Switzerland, 2013), Chap. 9.
  - [15] J.-F. Chang, T. Sakanoue, Y. Olivier, T. Uemura, M.-B. Dufourg-Madec, S. G. Yeates, J. Cornil, J. Takeya, A. Troisi, and H. Sirringhaus, *Phys. Rev. Lett.* **107**, 066601 (2011).

- [16] N. Martin, T. Nyberg, and V. Kapaklis, *Curr. Appl. Phys.* **14**, 1481 (2014).
- [17] M. Yamagishi, J. Soeda, T. Uemura, Y. Okada, Y. Takatsuki, T. Nishikawa, Y. Nakazawa, I. Doi, K. Takimiya, and J. Takeya, *Phys. Rev. B* **81**, 161306(R) (2010).
- [18] C.-G. Lee, B. Cob, and A. Dodabalapur, *Appl. Phys. Lett.* **97**, 203505 (2010).
- [19] S. Tomai, M. Nishimura, M. Itose, M. Matuura, M. Kasami, S. Matsuzaki, H. Kawashima, F. Utsuno, and K. Yano, *Jpn. J. Appl. Phys.* **51**, 03CB01 (2012).
- [20] S. M. Sze, *Physics of Semiconductor Devices*, 2nd ed. (Wiley, New York, 1981).
- [21] T. Kamiya, K. Nomura, and H. Hosono, *Appl. Phys. Lett.* **96**, 122103 (2010).
- [22] B. I. Shklovskii and A. L. Efros, *Electronic Processes of Doped Semiconductors* (Springer-Verlag, Berlin, 1984).
- [23] S. Kirkpatrick, *Rev. Mod. Phys.* **45**, 574 (1973).
- [24] I. I. Fishchuk, D. Hertel, H. Bässler, and A. Kadashchuk, *Phys. Rev. B* **65**, 125201 (2002).
- [25] I. I. Fishchuk, A. K. Kadashchuk, J. Genoe, M. Ullah, H. Sitter, Th. B. Singh, N. S. Sariciftci, and H. Bässler, *Phys. Rev. B* **81**, 045202 (2010).
- [26] I. I. Fishchuk, A. Kadashchuk, S. T. Hoffmann, S. Athanasopoulos, J. Genoe, H. Bässler, and A. Köhler, *Phys. Rev. B* **88**, 125202 (2013).
- [27] I. I. Fishchuk, A. Kadashchuk, A. Mityashin, M. M. Gavriluyk, A. Köhler, H. Bässler, J. Genoe, H. Sitter, and N. S. Sariciftci, *Phys. Rev. B* **90**, 245201 (2014).
- [28] E. O. Kane, *Phys. Rev.* **131**, 79 (1963).
- [29] H. Hosono, *J. Non-Cryst. Solids* **352**, 851 (2006).
- [30] P. K. Nayak, M. N. Hedhili, D. Cha, and H. N. Alshareef, *Appl. Phys. Lett.* **100**, 202106 (2012).
- [31] M. J. Powell, *IEEE Trans. Electron Devices* **36**, 2753 (1989).
- [32] Y. Ukai, *SID Dig. Tech. Pap.* **44**, 28 (2013).
- [33] T. Kamiya, K. Nomura, and H. Hosono, *J. Disp. Technol.* **5**, 462 (2009).
- [34] Y. W. Jeon, S. Kim, S. Lee, D. M. Kim, D. H. Kim, J. Park, C. J. Kim, I. Song, Y. Park, U.-I. Chung, J.-H. Lee, B. D. Ahn, S. Y. Park, J.-H. Park, and J. H. Kim, *IEEE Trans. Electron Devices* **57**, 2988 (2010).
- [35] M. Nardone, M. Simon, I. V. Karpov, and V. G. Karpov, *J. Appl. Phys.* **112**, 071101 (2012).
- [36] I. Zvyagin, in *Charge Transport in Disordered Solids with Applications in Electronics*, edited by S. Baranovski (John Wiley and Sons, Ltd., Chichester, UK, 2006).
- [37] S.M. Ryvkin and I. S. Shlimak, *Phys. Status Solidi A* **16**, 515 (1973).
- [38] J. A. Howard and R. A. Street, *Phys. Rev. B* **44**, 7935 (1991).
- [39] P. Bozsoki, S. D. Baranovskii, P. Thomas, and S. C. Agarwal, *Phys. Status Solidi C* **1**, 113 (2004).
- [40] D. Adler, L. P. Flora, and S. D. Senturia, *Solid State Commun.* **12**, 9 (1973).
- [41] E. J. Meijer, E. J. Meijer, M. Matters, P. T. Herwig, D. M. de Leeuw, and T. M. Klapwijk, *Appl. Phys. Lett.* **76**, 3433 (2000).
- [42] M. Ullah, I. I. Fishchuk, A. K. Kadashchuk, P. Stadler, A. Pivrikas, C. Simbrunner, V. N. Poroshin, N. S. Sariciftci, and H. Sitter, *Appl. Phys. Lett.* **96**, 213306 (2010).
- [43] S. K. Ram, S. Kumar, and P. Roca i Cabarrocas, *Phys. Rev. B* **77**, 045212 (2008).
- [44] R. Flukiger, J. Meier, M. Goetz, and A. Shah, *J. Appl. Phys.* **77**, 712 (1995).
- [45] M. Kondo, Y. Chida, and A. Matsuda, *J. Non-Cryst. Solids* **198–200**, 178 (1996).
- [46] M. H. Cohen and J. Jortner, *Phys. Rev. Lett.* **30**, 696 (1973).
- [47] D. Stroud, *Phys. Rev. B* **12**, 3368 (1975).
- [48] T. Uemura, M. Yamagishi, J. Soeda, Y. Takatsuki, Y. Okada, Y. Nakazawa, and J. Takeya, *Phys. Rev. B* **85**, 035313 (2012).
- [49] D. Vanderbilt, *Phys. Rev. B* **41**, 7892. (1990).
- [50] P. Giannozzi, S. Baroni, N. Bonini, M. Calandra, R. Car, C. Cavazzoni, D. Ceresoli, G. L. Chiarotti, M. Cococcioni, I. Dabo, A. Dal Corso, S. de Gironcoli, S. Fabris, G. Fratesi, R. Gebauer, U. Gerstmann, C. Gougoussis, A. Kokalj, M. Lazzeri, L. Martin-Samos *et al.*, *J. Phys.: Condens. Matter* **21**, 395502 (2009).
- [51] J. P. Perdew, K. Burke, and M. Ernzerhof, *Phys. Rev. Lett.* **77**, 3865 (1996).
- [52] S. Plimpton, *J. Comput. Phys.* **117**, 1 (1995).
- [53] R. Car and M. Parrinello, *Phys. Rev. Lett.* **60**, 204 (1988).
- [54] M. Orita, H. Tanji, M. Mizuno, H. Adachi, and I. Tanaka, *Phys. Rev. B* **61**, 1811 (2000).
- [55] A. de Jamblinne de Meux, G. Pourtois, J. Genoe, and P. Heremans, *J. Phys. D: Appl. Phys.* **48**, 435104 (2015).
- [56] T. Kamiya, K. Nomura, M. Hirano, and H. Hosono, *Phys. Status Solidi C* **5**, 3098 (2008).
- [57] A. Takagi, K. Nomura, H. Ohta, H. Yanagi, T. Kamiya, M. Hirano, and H. Hosono, *Thin Solid Films* **486**, 38 (2005).
- [58] K. Nomura, T. Kamiya, H. Yanagi, E. Ikenaga, K. Yang, K. Kobayashi, and H. Hosono, *Appl. Phys. Lett.* **92**, 202117 (2008).
- [59] K. Lee, K. Nomura, H. Yanagi, T. Kamiya, E. Ikenaga, T. Sugiyama, K. Kobayashi, and H. Hosono, *J. Appl. Phys.* **112**, 033713 (2012).
- [60] M. Nag, A. Bhoolakam, S. Steudel, A. Chasin, K. Myny, J. Maas, G. Groeseneken, and P. Heremans, *Jpn. J. Appl. Phys.* **53**, 111401 (2014).
- [61] E. A. Schiff, *J. Phys.: Condens. Matter* **16**, S5265 (2004).
- [62] J. Jeong, J. K. Jeong, J.-S. Park, Y.-G. Mo, and Y. Hong, *Jpn. J. Appl. Phys.* **49**, 03CB02 (2010).
- [63] H. Böttger and V. V. Bryksin, *Phys. Status Solidi B* **78**, 415 (1976).
- [64] L. Friedman and M. Pollak, *Philos. Mag. B* **38**, 173 (1978).
- [65] D. Emin, *Ann. Phys.* **64**, 336 (1971).
- [66] D. Emin, *Philos. Mag.* **35**, 1189 (1977).
- [67] P. G. Le Comber, D. I. Jones, and W. E. Spear, *Philos. Mag.* **35**, 1173 (1977).
- [68] W. Chr. Germs, W. H. Adriaans, A. K. Tripathi, W. S. C. Roelofs, B. Cobb, R. A. J. Janssen, G. H. Gelinck, and M. Kemerink, *Phys. Rev. B* **86**, 155319 (2012).